Pattern Anal Applic
DOI 10.1007/s10044-012-0266-x

THEORETICAL ADVANCES

# Adaptive edge-preserving image denoising using wavelet transforms

**Ricardo Dutra da Silva · Rodrigo Minetto · William Robson Schwartz · Helio Pedrini**

Received: 18 January 2011 / Accepted: 13 January 2012


**Abstract** Image denoising is a relevant issue found in diverse image processing and computer vision problems. It is a challenge to preserve important features, such as edges, corners and other sharp structures, during the denoising process. Wavelet transforms have been widely used for image denoising since they provide a suitable basis for separating noisy signal from the image signal. This paper describes a novel image denoising method based on wavelet transforms to preserve edges. The decomposition is performed by dividing the image into a set of blocks and transforming the data into the wavelet domain. An adaptive thresholding scheme based on edge strength is used to effectively reduce noise while preserving important features of the original image. Experimental results, compared to other approaches, demonstrate that the proposed method is suitable for different classes of images contaminated by Gaussian noise.

**Keywords** Image denoising · Wavelet transforms · Adaptive denoising · Edge preservation

## 1 Introduction

Digital images can be corrupted by noise during the process of acquisition and transmission, degrading their quality. A major challenge is to remove as much as possible of the noise without eliminating the most representative characteristics of the image, such as edges, corners and other sharp structures.

R. D. da Silva · R. Minetto · W. R. Schwartz (✉) · H. Pedrini
Institute of Computing, University of Campinas,
Campinas, SP 13083-852, Brazil
e-mail: schwartz@ic.unicamp.br

Several approaches [1–5] have been proposed to suppress the presence of noise in digital images, many of them based on spatial filters. These filters usually smooth the data to reduce noise effects; however, this process can cause image blurring or edge removal [3].

Many techniques for improving spatial filters have been developed by removing the noise more effectively while preserving edges in the data. Some of these techniques are based on partial differential equations and computational fluid dynamics such as level set methods [6], total variation (TV) methods [7–9], non-linear isotropic and anisotropic diffusion [10–12] and essentially non-oscillatory schemes [13]. Other methods combine impulse removal filters with local adaptive filtering in the transform domain to suppress noise [14]. Non-local filtering strategies have demonstrated great potential, in particular, the transform-based BM3D filter [15]. Singular value decomposition (SVD) is also used in image noise filtering [16, 17]. Cross-validation techniques are used for thresholding parameter selection [18, 19]. Bayesian procedures [20–22] combine inference from data with prior information to estimate thresholding parameters. Other techniques have combined wavelets with hidden Markov models and spatially adaptive methods [23–28]. A different class of methods exploits the decomposition of the data into a wavelet basis and modifies the wavelet coefficients to denoise the data [29–39].

The common idea related to the suppression of noise based on the wavelet transform is to compute the wavelet decomposition of the noisy image and to manipulate the obtained wavelet coefficients [40]. Coefficients that are supposed to be affected by noise are replaced by zero or an adequate value. Reconstruction from these manipulated coefficients then generates the resulting denoised image.

This paper describes a new method for noise suppression using wavelet transforms. An adaptive thresholding

Published online: 03 February 2012

that combines local processing and edge strength is used to effectively reduce Gaussian noise while preserving important features of the original image. Experimental results demonstrate that the proposed method, when compared to well-known denoising approaches, is suitable for different classes of images contaminated by noise.

The paper is organized as follows. Section 2 gives a brief review of wavelet thresholding. In Sect. 3, the proposed method is presented in details. Experimental results, including a comparison with other denoising methods, are given in Sect. 4. Finally, some discussions and conclusions are summarized in Sect. 5.

## 2 Image denoising by wavelet thresholding

Wavelet thresholding is a common approach for denoising due to its simplicity. There are several studies on thresholding the wavelet coefficients [23, 30, 32, 33, 38, 41]. The process, commonly called wavelet shrinkage, consists of the following main stages:

1. perform the discrete wavelet transform;
2. estimate a threshold;
3. apply the threshold according to a shrinkage rule;
4. perform the inverse wavelet transform using the thresholded coefficients.

Suppose that a given image $\mathbf{f} = \{f_{x,y}, x = 1, \ldots, M, y = 1, \ldots, N\}$ has been corrupted by additive noise according to the following model

$$\mathbf{g} = \mathbf{f} + \mathbf{n} \tag{1}$$

where $\mathbf{n}$ represents the noise and $\mathbf{g}$ the observed image. A common assumption is that the noise is statistically independent and identically distributed. Most of the existing methods are designed for the case of additive white Gaussian noise.

The decomposition of the image $\mathbf{g}$ into coefficients through a discrete wavelet transform $W$ can be expressed as

$$\mathbf{G} = W(\mathbf{g}) \tag{2}$$

The application of the discrete wavelet transform decomposes the input image into different frequency subbands, labeled as $\mathrm{LL}_J$, $\mathrm{LH}_k$, $\mathrm{HL}_k$ and $\mathrm{HH}_k$, $k = 1, 2, \ldots, J$, where the subscript indicates the $k$-th resolution level of wavelet transform and $J$ is the largest scale in the decomposition. These subbands contain different information about the image. The lowest frequency $\mathrm{LL}_J$ subband, obtained by low-pass filtering along the $x$ and $y$ directions, corresponds to a coarse approximation of the image signal. The $\mathrm{LH}_k$, $\mathrm{HL}_k$ and $\mathrm{HH}_k$ subbands correspond to horizontal, vertical and diagonal details of the image signal, respectively. The highest frequency $\mathrm{HH}_1$ subband can contain a significant amount of noise. The $\mathrm{LL}_{k-1}$ subband can be further recursively decomposed to form the $\mathrm{LH}_k$, $\mathrm{HL}_k$ and $\mathrm{HH}_k$ subbands.

After the selection of a threshold, the wavelet coefficients are modified according to a shrinkage function $T$, such that

$$\hat{\mathbf{F}} = T(\mathbf{G}) \tag{3}$$

The last step in the wavelet shrinkage is to transform the thresholded coefficients back to the original domain, expressed as

$$\hat{\mathbf{f}} = W^{-1}(\hat{\mathbf{F}}) \tag{4}$$

where $W^{-1}$ denotes the inverse discrete wavelet transform and $\hat{\mathbf{f}}$ is the denoised image.

### 2.1 Threshold estimation

A great challenge in the wavelet shrinkage process is to find an adequate threshold value. A small threshold will hold the majority of the coefficients associated with the noisy signal, then resulting in a signal that may still be noisy. On the other hand, a large threshold will shrink more coefficients, leading to a smoothing of the signal that may suppress important features of the image.

Three threshold estimation criteria, called VisuShrink, SureShrink and BayesShrink, are described as follows.

VisuShrink is a thresholding scheme that uses a single universal threshold proposed by Donoho and Johnstone [32], defined as

$$\lambda_V = \hat{\sigma}_{\text{noise}} \sqrt{2 \log L} \tag{5}$$

where $\hat{\sigma}^2_{\text{noise}}$ is the estimated noise deviation and $L = M \times N$ is the number of pixels in the image. The same threshold is applied to all levels of decomposition. Although the resulting estimate is very smooth and has a pleasant visual appearance, it is known that VisuShrink tends to oversmooth the signal [42].

SureShrink is a thresholding scheme that applies a subband adaptive threshold [33]. A separate threshold is computed for each subband based on Stein's unbiased risk estimator (SURE)

$$\lambda_S = \arg\min_{t \geq 0} \mathrm{SURE}(t, \mathbf{G}_S) \tag{6}$$

which minimizes the risk

$$\mathrm{SURE}(t, \mathbf{G}_S) = N_S - 2[1 : N_S] + \sum_{x,y=1}^{N_S} [\min(|G_{xy}|, t)]^2 \tag{7}$$

where $\mathbf{G}_S$ is the detail coefficients from subband $S$ and $N_S$ is the number of coefficients $G_{xy}$ in $\{\mathbf{G}_S\}$. As pointed out by Donoho and Johnstone [33], when the coefficients are

not very sparse, SureShrink is applied; if not, universal threshold is applied.

BayesShrink uses a Bayesian mathematical framework and assumes generalized Gaussian distribution for the wavelet coefficients in each detail subband to find the threshold that minimizes the Bayesian risk [20, 30], expressed as

$$\lambda_B = \frac{\hat{\sigma}^2_{\text{noise}}}{\hat{\sigma}_{\text{signal}}} = \frac{\hat{\sigma}^2_{\text{noise}}}{\sqrt{\max(\hat{\sigma}^2_{\mathbf{G}} - \hat{\sigma}^2_{\text{noise}}, 0)}} \tag{8}$$

where $\hat{\sigma}^2_{\mathbf{G}} = \frac{1}{N_S}\sum_{x,y=1}^{N_S} G^2_{xy}$ and $N_S$ is the number of wavelet coefficients $G_{xy}$ on the subband under consideration.

As in the previous equations, most thresholding algorithms require an estimate of the noise variance.

For images, the noise level can be estimated from the highest frequency coefficients. A robust estimate of noise variance uses the median absolute value of the wavelet coefficients [32], which is insensitive to isolated outliers of potentially high amplitudes, defined as

$$\hat{\sigma}_{\text{noise}} = \frac{\text{median}(|\text{G}_{\text{xy}}|)}{0.6745}, \quad G_{xy} \in \text{subband HH} \tag{9}$$

where $G_{xy}$ are the HH wavelet coefficients that form the finest decomposition level. It is assumed that the noise follows a Gaussian distribution with zero mean and variance $\sigma^2$.

### 2.2 Shrinkage rules

The shrinkage rule defines how the threshold must be applied. In its basic form, each coefficient in the wavelet transform domain is compared against a threshold. If the coefficient is smaller than the threshold, it is assigned zero; otherwise, it is kept or modified. The motivation is that large coefficients are due to important signal features, while small coefficients can be thresholded without affecting the significant features of the image.

One of the first works that describe such an approach was reported by Weaver et al. [39]. Donoho and Johnstone [32, 33, 41, 43] developed a systematic theory for wavelet thresholding. Jansen [44] and Antoniadis [45] extensively reviewed wavelet thresholding techniques for image noise reduction.

In the shrinkage rule known as hard thresholding, the coefficients $w = G_{xy}$ that are less than or equal to the threshold $\lambda$ are set to zero, while the remaining coefficients are left unchanged

$$T_{\text{hard}}(w) = \begin{cases} w, & \text{if } |w| > \lambda \\ 0, & \text{if } |w| \le \lambda \end{cases} \tag{10}$$

In soft thresholding, the wavelet coefficients above the threshold are reduced by an amount equal to the value of the threshold

$$T_{\text{soft}}(w) = \begin{cases} \text{sgn}(w)(|w| - \lambda)_+, & \text{if } |w| > \lambda \\ 0, & \text{if } |w| \le \lambda \end{cases} \tag{11}$$

where $\text{sgn}(x)$ function returns the sign of the parameter $x$ and $(a)_+$ is defined as

$$(a)_+ = \begin{cases} 0, & \text{if } a < 0 \\ a, & \text{if } a \ge 0 \end{cases} \tag{12}$$

A disadvantage of the hard thresholding is its abrupt discontinuity, which may cause artifacts in the reconstructed image. On the other hand, the soft thresholding tends to oversmooth the reconstructed image.

Other thresholding schemes have been proposed, which are a compromise between the two previous approaches. The hyperbola function is continuous and attenuates large coefficients less than soft thresholding [22].

$$T_{\text{hyper}}(w) = \begin{cases} \text{sgn}(w)\sqrt{w^2 - \lambda^2}, & \text{if } |w| > \lambda \\ 0, & \text{if } |w| \le \lambda \end{cases} \tag{13}$$

Gao et al. [46] proposed the firm thresholding to avoid the drawbacks of both hard and soft thresholding rules, providing less sensitivity to small perturbations in the data and smaller overall mean-squared error, given by

$$T_{\text{firm}}(w) = \begin{cases} w, & \text{if } |w| > \lambda_2 \\ \text{sgn}(w)\frac{\lambda_2(|w| - \lambda_1)}{\lambda_2 - \lambda_1}, & \text{if } \lambda_1 < |w| \le \lambda_2 \\ 0, & \text{if } |w| \le \lambda_1 \end{cases} \tag{14}$$

The firm thresholding requires two threshold values, $\lambda_1$ and $\lambda_2$, making the estimation procedure more computationally expensive. To overcome this drawback, Gao et al. [47] proposed the nonnegative garrote thresholding

$$T_{\text{garrote}}(w) = \begin{cases} w - \frac{\lambda^2}{w}, & \text{if } |w| > \lambda \\ 0, & \text{if } |w| \le \lambda \end{cases} \tag{15}$$

which offers advantages over hard and soft thresholding and is comparable to the firm thresholding, while requiring only one threshold value.

Antoniadis and Fan [48] suggested the SCAD thresholding rule, defined as

$$T_{\text{SCAD}}(w) = \begin{cases} w, & \text{if } |w| > \alpha\lambda \\ \frac{(\alpha-1)w - \alpha\lambda\text{sgn}(w)}{\alpha - 2}, & \text{if } 2\lambda < |w| \le \alpha\lambda \\ \text{sgn}(w)\max(0, |w| - \lambda), & \text{if } |w| \le 2\lambda \end{cases} \tag{16}$$

where the authors recommended the use of $\alpha = 3.7$.

## 3 Image denoising method

In conventional thresholding schemes, a global (universal) threshold is commonly used to filter small wavelet coefficients. However, this procedure can also remove high-frequency components, such as edges. To improve the

wavelet denoising method, an adaptive threshold is calculated in a subband-dependent manner to characterize local features of the image. A new thresholding scheme is proposed to threshold the small wavelet coefficients considered to be noise while preserving edges. This subband-dependent thresholding is obtained based on the calculation of noise level and edge strength. The main stages of the proposed wavelet denoising method are illustrated in Fig. 1.

Initially, the input image **g**, corrupted by Gaussian noise, is partitioned into $m \times m$ pixel blocks. Blocks are used in a manner such that the denoising algorithm can exploit local noise characteristics and adapt thresholding to produce better results. Nevertheless, as information is often lost due to the thresholding, blocking effects between boundaries of neighbor blocks often arise. A larger region $B_n$ of size $n \times n$ pixels ($n > m$), encompassing an $m \times m$ block $B_m$, is used to avoid such undesirable effects. The discrete wavelet transform is then applied to each block $B_n$.

An edge detection algorithm is used to identify edges in the image. A multiscale edge detection based on Haar wavelet transform modulus maxima is used for this purpose [49], being applied separately to each block. In order to have a precise edge localization and avoid noise, after applying the edge detection, each coefficient identified as edge information is compared to its neighbors. If there is no neighbor belonging to an edge, the coefficient is no longer identified as edge information. The multiscale edge detection produces an edge map for each subband, that is, a binary image where 1 represents an active edge element and 0 represents a non-edge element.

The threshold on a given subband $i$ is given by

$$\lambda_i = \frac{\hat{\sigma}^2_{\text{noise}}}{\hat{\sigma}_{\text{signal,i}}} \tag{17}$$

where $\hat{\sigma}^2_{\text{noise}}$ is the local estimated noise variance, as in Eq. 9, considering the HH subband at the same decomposition level as the $i$ subband, and $\hat{\sigma}_{\text{signal},i}$ is the local estimated signal deviation on the subband under consideration, estimated as

$$\hat{\sigma}_{\text{signal},i} = \sqrt{\max(\hat{\sigma}^2_{\mathbf{G}} - \hat{\sigma}^2_{\text{noise}}, 0)} \tag{18}$$

where $\hat{\sigma}^2_{\mathbf{G}} = \frac{1}{N_S}\sum_{x,y=1}^{N_S} G^2_{xy}$ and $N_S$ is the number of wavelet coefficients $G_{xy}$ on the subband under consideration.

Therefore, the wavelet coefficients are thresholded adaptively according to their subbands. As the decomposition level increases, the coefficients of the subband usually become smoother. For example, the subband $HH_3$ is smoother than the corresponding subband in the previous level ($HH_2$), so the threshold value of $HH_3$ should be estimated to remove fewer coefficients than the one for $HH_2$.

A shrinkage rule is applied taking into account the threshold according to the edge map. Coefficients related to active edge elements must be associated with smaller threshold values. For such coefficients, the threshold $\lambda_c$ proposed in our method is computed as the product between the subband threshold $\lambda_i$ and a given value $\tau$, expressed by

$$\lambda_c = \tau\lambda_i \tag{19}$$

that is, $\tau$ corresponds to a factor used to weight the threshold in wavelet coefficients related to edges in the image.

Finally, the inverse multiscale decomposition is performed over each external block $B_n$. The non-overlapping inner blocks $B_m$ are used to reconstruct the denoised image $\hat{\mathbf{f}}$ and reduce errors near block boundaries, since the blocks $B_m$, when concatenated, are much less likely to suffer blocking effects.

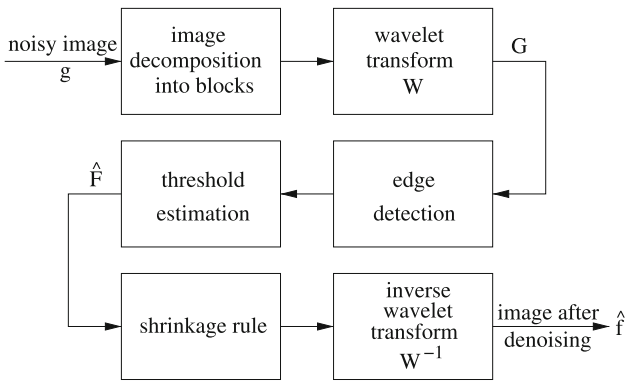


**Fig. 1** Diagram of the proposed denoising method

## 4 Experimental results

The proposed image denoising method, implemented in Matlab, is applied to several test images corrupted with additive Gaussian noise $N(0, \sigma^2)$. The test set comprises images form Caltech 256 database [50], as well as well-known images such as *glasses, lightning, window, boat, fingerprint* and *man*. A subset of the images, shown in Fig. 2, is considered in the discussions that follows. Experimental results at different noise levels are reported. The following sections describe the used performance metrics, the experimental setup for the proposed method and comparisons to other denoising approaches.

### 4.1 Performance metrics

The ultimate objective of image denoising is to produce an estimate $\hat{\mathbf{f}}$ of the unknown noise-free image **f**, which

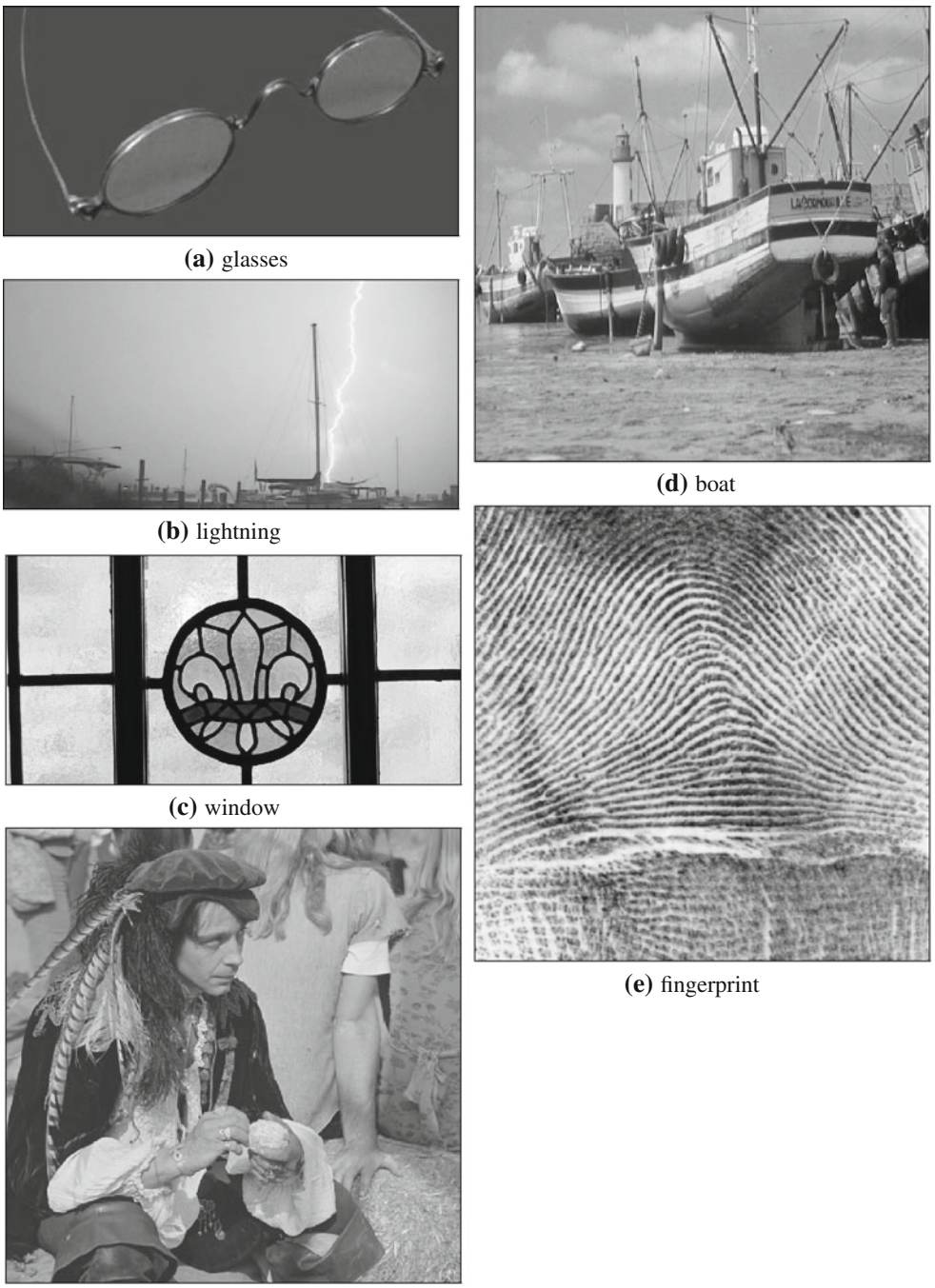

**(a)** glasses

**(b)** lightning

**(c)** window

**(d)** boat

**(e)** fingerprint

**(f)** man

**Fig. 2** Images used in the comparisons

approximates it best, under given evaluation criteria. A common criterion is minimizing the mean-squared error (MSE), which is defined for gray-scale images as

$$\mathrm{MSE} = \frac{1}{M \times N} ||\mathbf{f} - \hat{\mathbf{f}}||^2 = \frac{1}{M \times N} \sum_{x=1}^{M} \sum_{y=1}^{N} (f_{xy} - \hat{f}_{xy})^2. \quad (20)$$

Another common performance measure based on MSE is the peak signal to noise ratio (PSNR), which is defined in decibels (dB) for 8-bit gray-scale images as

$$\mathrm{PSNR} = 10 \log_{10} \left( \frac{255^2}{\mathrm{MSE}} \right). \quad (21)$$

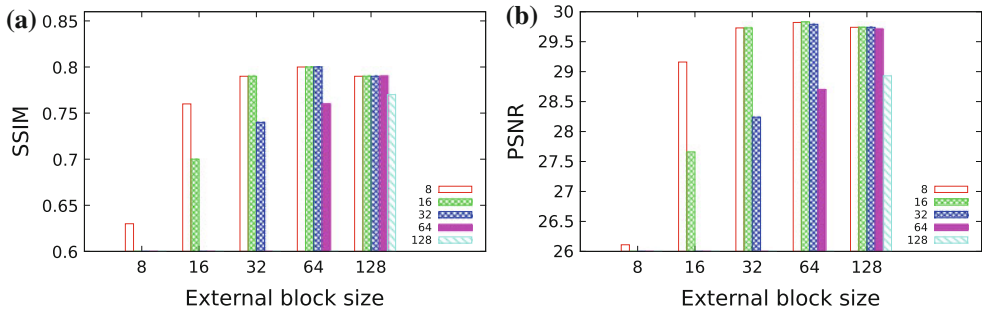


**Fig. 3** Comparison results for different block sizes. Each set of grouped bars corresponds to multiple inner blocks for a fixed external block size

A critical issue with the MSE (or PSNR) is that it does not measure the resulting image quality directly and it can attribute similar scores to images with large differences in psychovisual quality. The structural similarity index (SSIM) [51] was proposed as a metric to compare images which correlates more appropriately with the human perception. It maps two images into an index in the interval $[-1, 1]$, where higher values are given to more similar pairs of images $A$ and $B$, calculated as

$$\mathrm{SSIM}(A,B) = \frac{(2\mu_A\mu_B + c_1)(2\sigma_{AB} + c_2)}{(\mu_A^2 + \mu_B^2 + c_1)(\sigma_A^2 + \sigma_B^2 + c_2)} \tag{22}$$

where $\mu_A$, $\mu_B$, $\sigma_A^2$ and $\sigma_B^2$ are the averages and variances of $A$ and $B$, $\sigma_{AB}$ is the covariance between $A$ and $B$, and both $c_1$ and $c_2$ are predefined constants.

Pratt's figure of merit (FOM) [52] is widely employed to objectively rate the quality of edge detection, defined as

$$\mathrm{FOM} = \frac{1}{\max(N_I, N_D)} \sum_{i=1}^{N_D} \frac{1}{1 + \alpha d_i^2} \tag{23}$$

where $N_I$ and $N_D$ are the numbers of ideal and detected edge pixels, respectively, $\alpha$ is an empirical constant (often 1/9) used to penalize displaced edges and $d_i$ represents the distance between an edge point and the nearest ideal edge pixel. The value of FOM is a number in the interval [0, 1], where 1 represents the better performance, that is, the detected edges coincide with the ideal edges.

## 4.2 Experimental setup

We estimate a set of parameters used by the proposed method: wavelet transform and its number of decomposition levels, block sizes, shrinkage rule and $\tau$ (Eq. 19). To perform these estimations, a set of images, different from those shown in the comparisons, was used. Once the parameters are set, they are kept fixed throughout the comparisons to other methods.

A set of stationary wavelets [53] from Symlet, Coiflet, Daubechies and Biorthogonal families is tested for effectiveness. According to our experiments, Daubechies-3 (db3) provided better results than other wavelet bases. Thus, all wavelet-based methods (Bayes, Bivariate, Adaptive) used the Daubechies-3 wavelet for comparison purpose. In addition, four decomposition levels achieved the best results and will be considered in the remaining experiments.

Different block sizes are considered in the experiments. Figures 3 and 4 show PSNR e SSIM responses for different block sizes, achieved by averaging the responses over multiple images and noise levels. Large blocks allow effective removal of low-frequency noise, but tend to smooth details. Tests revealed that blocks with sizes up to $64 \times 64$ pixels encompassing blocks sized a multiple of their size preserve sharp characteristics and avoid blockiness. Based on the results obtained, shown in Fig. 3, blocks of size $64 \times 64$ pixels encompassing blocks of size $16 \times 16$ provided slightly better results than the other block sizes (considering PSNR and SSIM) and will be used during the comparisons.

According to our experiments, the best value for $\tau$, defined in Eq. 19, is 0.8. This shows that it is worth having a trade-off between smoothness and edge preservation. This value will be used in the remaining experiments and comparisons.

Finally, a comparison among different shrinkage rules used in our denoising method is shown in Fig. 4. The PSNR value obtained for each shrinkage rule corresponds

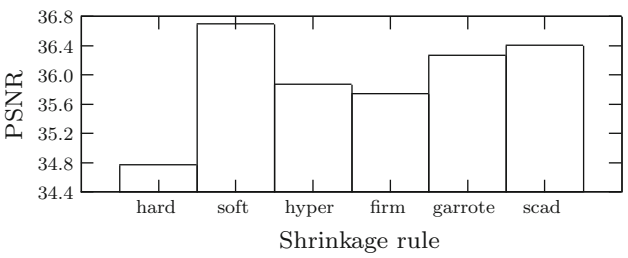


**Fig. 4** Comparison results for shrinkage rules

**Table 1** PSNR results for a set of test images and noise levels

| | Non wavelet-based methods | | | | | Wavelet-based methods | | | |
|---|---|---|---|---|---|---|---|---|---|
| | BM3D method | AD method | Median filter | TV method | Wiener filter | Bayes method | Bivariate method | Wiener-chop method | Proposed method |
| Glasses | | | | | | | | | |
| $\sigma = 10$ | **41.79** | 40.16 | 35.15 | 40.19 | 37.81 | 39.78 | 36.53 | 40.92 | 40.76 |
| $\sigma = 15$ | **40.64** | 37.65 | 31.92 | 37.80 | 34.82 | 37.19 | 34.40 | 38.20 | 38.80 |
| $\sigma = 20$ | **39.58** | 35.73 | 29.53 | 33.74 | 32.62 | 35.75 | 32.43 | 36.09 | 37.16 |
| $\sigma = 25$ | **38.67** | 34.47 | 27.68 | 30.27 | 31.05 | 34.81 | 30.90 | 34.74 | 36.17 |
| $\sigma = 30$ | **35.41** | 33.22 | 26.14 | 27.55 | 29.79 | 33.88 | 29.40 | 33.37 | 35.01 |
| $\sigma = 35$ | 30.21 | 32.13 | 24.81 | 25.34 | 28.64 | 33.09 | 28.20 | 32.27 | **34.05** |
| Lightning | | | | | | | | | |
| $\sigma = 10$ | 37.85 | **38.37** | 33.76 | 37.52 | 36.05 | 33.66 | 30.56 | 37.53 | 38.29 |
| $\sigma = 15$ | **37.17** | 35.99 | 31.04 | 35.79 | 33.78 | 32.11 | 29.87 | 35.05 | 36.15 |
| $\sigma = 20$ | **36.40** | 34.35 | 29.07 | 32.88 | 32.03 | 30.05 | 29.13 | 33.39 | 35.02 |
| $\sigma = 25$ | **35.62** | 33.05 | 27.32 | 29.87 | 30.46 | 29.31 | 28.27 | 32.14 | 34.09 |
| $\sigma = 30$ | **33.39** | 31.95 | 25.83 | 27.24 | 29.10 | 28.98 | 27.31 | 31.07 | 33.31 |
| $\sigma = 35$ | 28.76 | 30.97 | 24.60 | 25.17 | 27.91 | 28.04 | 26.43 | 30.16 | **32.54** |
| Window | | | | | | | | | |
| $\sigma = 10$ | 29.63 | **32.04** | 27.61 | 29.80 | 28.96 | 31.01 | 24.70 | 31.16 | 31.27 |
| $\sigma = 15$ | 29.34 | **30.14** | 26.82 | 29.45 | 28.13 | 29.17 | 24.41 | 29.59 | 29.60 |
| $\sigma = 20$ | **29.03** | 28.78 | 25.93 | 28.67 | 27.26 | 27.87 | 24.04 | 28.36 | 28.37 |
| $\sigma = 25$ | **28.62** | 27.62 | 25.06 | 27.49 | 26.37 | 26.74 | 23.61 | 27.30 | 27.36 |
| $\sigma = 30$ | **28.09** | 26.67 | 24.22 | 26.21 | 25.56 | 25.88 | 23.15 | 26.44 | 26.54 |
| $\sigma = 35$ | **26.71** | 25.72 | 23.36 | 24.83 | 24.64 | 24.96 | 22.61 | 25.59 | 25.71 |
| Boat | | | | | | | | | |
| $\sigma = 10$ | 31.02 | 32.33 | 29.40 | 30.39 | 30.02 | 30.47 | 26.79 | 32.20 | **32.52** |
| $\sigma = 15$ | 30.70 | 30.40 | 28.19 | 29.95 | 29.07 | 29.07 | 26.49 | 30.59 | **30.81** |
| $\sigma = 20$ | **30.30** | 28.98 | 26.94 | 28.81 | 28.06 | 27.97 | 26.09 | 29.33 | 29.43 |
| $\sigma = 25$ | **29.84** | 27.90 | 25.80 | 27.39 | 27.23 | 26.99 | 25.59 | 28.44 | 28.48 |
| $\sigma = 30$ | **28.61** | 26.97 | 24.69 | 25.72 | 26.35 | 26.18 | 25.00 | 27.60 | 27.66 |
| $\sigma = 35$ | 25.83 | 26.22 | 23.69 | 24.13 | 25.58 | 25.56 | 24.41 | 26.91 | **27.05** |
| Fingerprint | | | | | | | | | |
| $\sigma = 10$ | 29.05 | 30.46 | 29.10 | 28.76 | 24.89 | 31.17 | 25.84 | 31.51 | **31.67** |
| $\sigma = 15$ | 28.78 | 28.19 | 27.72 | 28.01 | 24.60 | 29.47 | 25.54 | 29.79 | **29.88** |
| $\sigma = 20$ | 28.38 | 26.51 | 26.48 | 26.89 | 24.23 | 28.00 | 25.15 | 28.38 | **28.48** |
| $\sigma = 25$ | **27.70** | 25.20 | 25.35 | 25.58 | 23.86 | 26.81 | 24.71 | 27.23 | 27.35 |
| $\sigma = 30$ | 26.31 | 24.17 | 24.34 | 24.32 | 23.51 | 25.84 | 24.25 | 26.33 | **26.46** |
| $\sigma = 35$ | 23.86 | 23.20 | 23.42 | 23.03 | 23.08 | 24.95 | 23.71 | 25.49 | **25.65** |
| Man | | | | | | | | | |
| $\sigma = 10$ | 30.39 | 32.56 | 30.20 | 30.72 | 30.50 | 31.22 | 28.16 | 32.09 | **32.34** |
| $\sigma = 15$ | 30.14 | 30.51 | 28.78 | 30.27 | 29.48 | 29.76 | 27.72 | 30.52 | **30.55** |
| $\sigma = 20$ | **29.93** | 29.18 | 27.43 | 29.23 | 28.55 | 28.74 | 27.18 | 29.43 | 29.38 |
| $\sigma = 25$ | **29.60** | 28.13 | 26.10 | 27.58 | 27.66 | 27.70 | 26.54 | 28.57 | 28.55 |
| $\sigma = 30$ | **28.46** | 27.31 | 24.95 | 25.88 | 26.81 | 26.99 | 25.87 | 27.80 | 27.82 |
| $\sigma = 35$ | 25.74 | 26.58 | 23.88 | 24.22 | 25.99 | 26.32 | 25.15 | 27.13 | **27.22** |

Values marked in bold indicate the best results among all compared methods and values with underline indicate the best results among the wavelet-based methods

**Table 2** SSIM results for a set of test images and noise levels

| | Non-wavelet based | | | | | Wavelet based | | | |
|---|---|---|---|---|---|---|---|---|---|
| | BM3D method | AD method | Median filter | TV method | Wiener filter | Bayes method | Bivariate method | Wiener-chop method | Proposed method |
| Glasses | | | | | | | | | |
| $\sigma = 10$ | **0.98** | 0.96 | 0.83 | 0.98 | 0.95 | 0.97 | 0.93 | 0.96 | 0.97 |
| $\sigma = 15$ | **0.98** | 0.94 | 0.70 | 0.95 | 0.89 | 0.95 | 0.86 | 0.93 | 0.96 |
| $\sigma = 20$ | **0.97** | 0.91 | 0.58 | 0.85 | 0.81 | 0.94 | 0.78 | 0.90 | 0.95 |
| $\sigma = 25$ | **0.96** | 0.88 | 0.48 | 0.68 | 0.74 | 0.94 | 0.71 | 0.87 | 0.94 |
| $\sigma = 30$ | 0.88 | 0.85 | 0.40 | 0.51 | 0.68 | **0.94** | 0.64 | 0.83 | 0.93 |
| $\sigma = 35$ | 0.62 | 0.81 | 0.34 | 0.38 | 0.62 | **0.93** | 0.58 | 0.80 | **0.93** |
| Lightning | | | | | | | | | |
| $\sigma = 10$ | **0.96** | 0.95 | 0.82 | 0.96 | 0.93 | 0.95 | 0.89 | 0.95 | 0.95 |
| $\sigma = 15$ | **0.95** | 0.92 | 0.70 | 0.93 | 0.89 | 0.93 | 0.83 | 0.91 | 0.94 |
| $\sigma = 20$ | **0.95** | 0.89 | 0.59 | 0.84 | 0.84 | 0.91 | 0.76 | 0.88 | 0.93 |
| $\sigma = 25$ | **0.94** | 0.86 | 0.49 | 0.68 | 0.77 | 0.90 | 0.69 | 0.85 | 0.92 |
| $\sigma = 30$ | 0.85 | 0.82 | 0.41 | 0.52 | 0.70 | 0.90 | 0.61 | 0.81 | **0.91** |
| $\sigma = 35$ | 0.57 | 0.79 | 0.35 | 0.39 | 0.63 | 0.89 | 0.55 | 0.78 | **0.90** |
| Window | | | | | | | | | |
| $\sigma = 10$ | 0.66 | **0.80** | 0.72 | 0.70 | 0.65 | 0.79 | 0.66 | 0.77 | 0.75 |
| $\sigma = 15$ | 0.64 | **0.72** | 0.66 | 0.70 | 0.61 | 0.71 | 0.61 | 0.71 | 0.68 |
| $\sigma = 20$ | 0.62 | 0.66 | 0.60 | **0.68** | 0.58 | 0.65 | 0.56 | 0.66 | 0.62 |
| $\sigma = 25$ | 0.62 | 0.61 | 0.54 | **0.64** | 0.55 | 0.61 | 0.51 | 0.61 | 0.58 |
| $\sigma = 30$ | **0.61** | 0.58 | 0.49 | 0.58 | 0.52 | 0.57 | 0.47 | 0.58 | 0.55 |
| $\sigma = 35$ | **0.57** | 0.54 | 0.44 | 0.52 | 0.50 | 0.54 | 0.44 | 0.55 | 0.53 |
| Boat | | | | | | | | | |
| $\sigma = 10$ | 0.82 | 0.85 | 0.78 | 0.80 | 0.78 | 0.84 | 0.74 | **0.86** | **0.86** |
| $\sigma = 15$ | 0.81 | 0.80 | 0.71 | 0.80 | 0.76 | 0.79 | 0.71 | **0.82** | 0.82 |
| $\sigma = 20$ | **0.81** | 0.76 | 0.65 | 0.76 | 0.73 | 0.75 | 0.68 | 0.79 | 0.79 |
| $\sigma = 25$ | **0.80** | 0.72 | 0.58 | 0.69 | 0.70 | 0.72 | 0.64 | 0.76 | 0.76 |
| $\sigma = 30$ | **0.76** | 0.69 | 0.52 | 0.60 | 0.67 | 0.69 | 0.59 | 0.72 | 0.73 |
| $\sigma = 35$ | 0.61 | 0.66 | 0.47 | 0.52 | 0.63 | 0.66 | 0.56 | 0.69 | **0.71** |
| Fingerprint | | | | | | | | | |
| $\sigma = 10$ | 0.92 | 0.95 | 0.93 | 0.92 | 0.83 | **0.96** | 0.87 | **0.96** | **0.96** |
| $\sigma = 15$ | 0.92 | 0.92 | 0.91 | 0.91 | 0.82 | **0.94** | 0.86 | **0.94** | **0.94** |
| $\sigma = 20$ | 0.92 | 0.88 | 0.89 | 0.90 | 0.81 | 0.92 | 0.85 | **0.93** | **0.93** |
| $\sigma = 25$ | **0.91** | 0.84 | 0.86 | 0.87 | 0.80 | 0.90 | 0.83 | **0.91** | **0.91** |
| $\sigma = 30$ | **0.89** | 0.81 | 0.84 | 0.84 | 0.79 | 0.87 | 0.82 | **0.89** | **0.89** |
| $\sigma = 35$ | 0.82 | 0.77 | 0.81 | 0.80 | 0.78 | 0.85 | 0.80 | **0.87** | **0.87** |
| Man | | | | | | | | | |
| $\sigma = 10$ | 0.82 | 0.87 | 0.81 | 0.82 | 0.81 | 0.87 | 0.78 | **0.88** | 0.87 |
| $\sigma = 15$ | 0.81 | 0.82 | 0.74 | 0.82 | 0.78 | 0.82 | 0.75 | **0.84** | 0.83 |
| $\sigma = 20$ | **0.81** | 0.77 | 0.67 | 0.78 | 0.75 | 0.79 | 0.71 | 0.80 | 0.79 |
| $\sigma = 25$ | **0.80** | 0.73 | 0.60 | 0.70 | 0.72 | 0.75 | 0.67 | 0.77 | 0.76 |
| $\sigma = 30$ | **0.75** | 0.70 | 0.53 | 0.60 | 0.68 | 0.72 | 0.63 | 0.73 | 0.74 |
| $\sigma = 35$ | 0.60 | 0.66 | 0.48 | 0.52 | 0.64 | 0.69 | 0.58 | 0.70 | **0.72** |

Values marked in bold indicate the best results among all compared methods and values with underline indicate the best results among the wavelet-based methods

**Table 3** FOM results for a set of test images and noise levels

| | Non-wavelet based | | | | | Wavelet based | | | |
|---|---|---|---|---|---|---|---|---|---|
| | BM3D method | AD method | Median filter | TV method | Wiener filter | Bayes method | Bivariate method | Wiener-chop method | Proposed method |
| Glasses | | | | | | | | | |
| $\sigma = 10$ | 0.77 | 0.82 | 0.81 | 0.75 | 0.80 | 0.76 | 0.69 | **0.86** | 0.85 |
| $\sigma = 15$ | 0.75 | 0.79 | 0.74 | 0.78 | 0.77 | 0.65 | 0.67 | **0.81** | 0.80 |
| $\sigma = 20$ | **0.76** | 0.73 | 0.62 | 0.72 | 0.69 | 0.61 | 0.64 | **0.76** | 0.74 |
| $\sigma = 25$ | **0.76** | 0.68 | 0.50 | 0.49 | 0.58 | 0.55 | 0.60 | 0.72 | 0.68 |
| $\sigma = 30$ | **0.80** | 0.72 | 0.42 | 0.39 | 0.53 | 0.57 | 0.59 | 0.66 | 0.69 |
| $\sigma = 35$ | **0.74** | 0.62 | 0.34 | 0.33 | 0.46 | 0.50 | 0.53 | 0.55 | 0.66 |
| Lightning | | | | | | | | | |
| $\sigma = 10$ | 0.75 | 0.81 | 0.68 | 0.68 | 0.65 | 0.62 | 0.54 | 0.80 | **0.82** |
| $\sigma = 15$ | **0.74** | 0.74 | 0.65 | 0.69 | 0.64 | 0.55 | 0.52 | **0.77** | **0.77** |
| $\sigma = 20$ | 0.72 | 0.68 | 0.59 | 0.68 | 0.62 | 0.46 | 0.52 | 0.71 | **0.73** |
| $\sigma = 25$ | **0.74** | 0.64 | 0.56 | 0.66 | 0.59 | 0.40 | 0.48 | 0.68 | 0.71 |
| $\sigma = 30$ | **0.76** | 0.62 | 0.52 | 0.55 | 0.58 | 0.39 | 0.49 | 0.63 | 0.68 |
| $\sigma = 35$ | **0.75** | 0.61 | 0.46 | 0.45 | 0.54 | 0.33 | 0.46 | 0.56 | 0.65 |
| Window | | | | | | | | | |
| $\sigma = 10$ | 0.97 | **0.99** | 0.86 | 0.93 | 0.92 | 0.96 | 0.72 | 0.96 | 0.98 |
| $\sigma = 15$ | **0.97** | 0.97 | 0.86 | 0.93 | 0.91 | 0.93 | 0.71 | 0.94 | 0.96 |
| $\sigma = 20$ | **0.97** | 0.96 | 0.85 | 0.92 | 0.89 | 0.92 | 0.71 | 0.93 | 0.96 |
| $\sigma = 25$ | **0.97** | 0.94 | 0.85 | 0.92 | 0.89 | 0.91 | 0.71 | 0.93 | 0.95 |
| $\sigma = 30$ | **0.97** | 0.92 | 0.83 | 0.91 | 0.87 | 0.88 | 0.70 | 0.92 | 0.94 |
| $\sigma = 35$ | **0.97** | 0.90 | 0.83 | 0.90 | 0.87 | 0.87 | 0.70 | 0.91 | 0.93 |
| Boat | | | | | | | | | |
| $\sigma = 10$ | 0.85 | **0.95** | 0.74 | 0.80 | 0.78 | 0.78 | 0.56 | 0.85 | 0.87 |
| $\sigma = 15$ | 0.86 | **0.88** | 0.71 | 0.80 | 0.75 | 0.73 | 0.55 | 0.80 | 0.82 |
| $\sigma = 20$ | **0.85** | 0.81 | 0.68 | 0.78 | 0.72 | 0.67 | 0.54 | 0.76 | 0.77 |
| $\sigma = 25$ | **0.88** | 0.77 | 0.65 | 0.75 | 0.70 | 0.61 | 0.53 | 0.75 | 0.75 |
| $\sigma = 30$ | **0.85** | 0.72 | 0.59 | 0.69 | 0.65 | 0.55 | 0.52 | 0.71 | 0.71 |
| $\sigma = 35$ | **0.82** | 0.68 | 0.55 | 0.65 | 0.63 | 0.50 | 0.49 | 0.68 | 0.68 |
| Fingerprint | | | | | | | | | |
| $\sigma = 10$ | 0.88 | 0.87 | **0.89** | 0.86 | 0.89 | 0.74 | 0.58 | 0.75 | 0.79 |
| $\sigma = 15$ | 0.86 | 0.85 | **0.88** | 0.85 | 0.88 | 0.71 | 0.57 | 0.73 | 0.74 |
| $\sigma = 20$ | **0.86** | 0.83 | 0.85 | 0.83 | 0.85 | 0.68 | 0.55 | 0.71 | 0.72 |
| $\sigma = 25$ | **0.86** | 0.81 | 0.82 | 0.80 | 0.83 | 0.67 | 0.53 | 0.71 | 0.72 |
| $\sigma = 30$ | **0.82** | 0.80 | 0.77 | 0.78 | 0.82 | 0.62 | 0.51 | 0.70 | 0.70 |
| $\sigma = 35$ | 0.78 | 0.78 | 0.72 | 0.76 | **0.80** | 0.59 | 0.52 | 0.70 | 0.71 |
| Man | | | | | | | | | |
| $\sigma = 10$ | 0.74 | **0.92** | 0.75 | 0.79 | 0.76 | 0.78 | 0.57 | 0.82 | 0.82 |
| $\sigma = 15$ | 0.74 | 0.83 | 0.69 | 0.78 | 0.72 | 0.71 | 0.56 | **0.78** | 0.76 |
| $\sigma = 20$ | **0.75** | 0.77 | 0.66 | 0.76 | 0.69 | 0.66 | 0.55 | 0.74 | 0.72 |
| $\sigma = 25$ | **0.78** | 0.73 | 0.62 | 0.74 | 0.68 | 0.58 | 0.53 | 0.73 | 0.70 |
| $\sigma = 30$ | **0.79** | 0.68 | 0.58 | 0.69 | 0.64 | 0.53 | 0.52 | 0.69 | 0.66 |
| $\sigma = 35$ | **0.79** | 0.67 | 0.53 | 0.65 | 0.62 | 0.47 | 0.50 | 0.67 | 0.63 |

Values marked in bold indicate the best results among all compared methods and values with underline indicate the best results among the wavelet-based methods

to an average calculated over a subset of all images used in our experiments. The soft shrinkage rule, given in Eq. 11, is clearly superior to other schemes and, therefore, it is chosen over other described rules to threshold coefficients in our experiments.

### 4.3 Comparisons

To assess the denoising effectiveness, the proposed method is compared to state-of-the-art methods. Namely, Bayes [30], Bivariate [38] and Wiener-chop [34], which are


**Fig. 5** Denoising results for image man

wavelet-based; and median, Wiener, BM3D [15], anisotropic diffusion (AD) [11] and TV [9], which are non wavelet-based. PSNR (in dB), SSIM and FOM values of the denoised images relative to their original images using such methods are reported in Tables 1, 2 and 3, respectively. The best values for wavelet-based and non wavelet-based methods are highlighted with underline and boldface, respectively.

The four right-most columns in each table show the results of wavelet-based denoising methods. The results obtained by the proposed method reveal significant gain when compared with such methods, specially considering

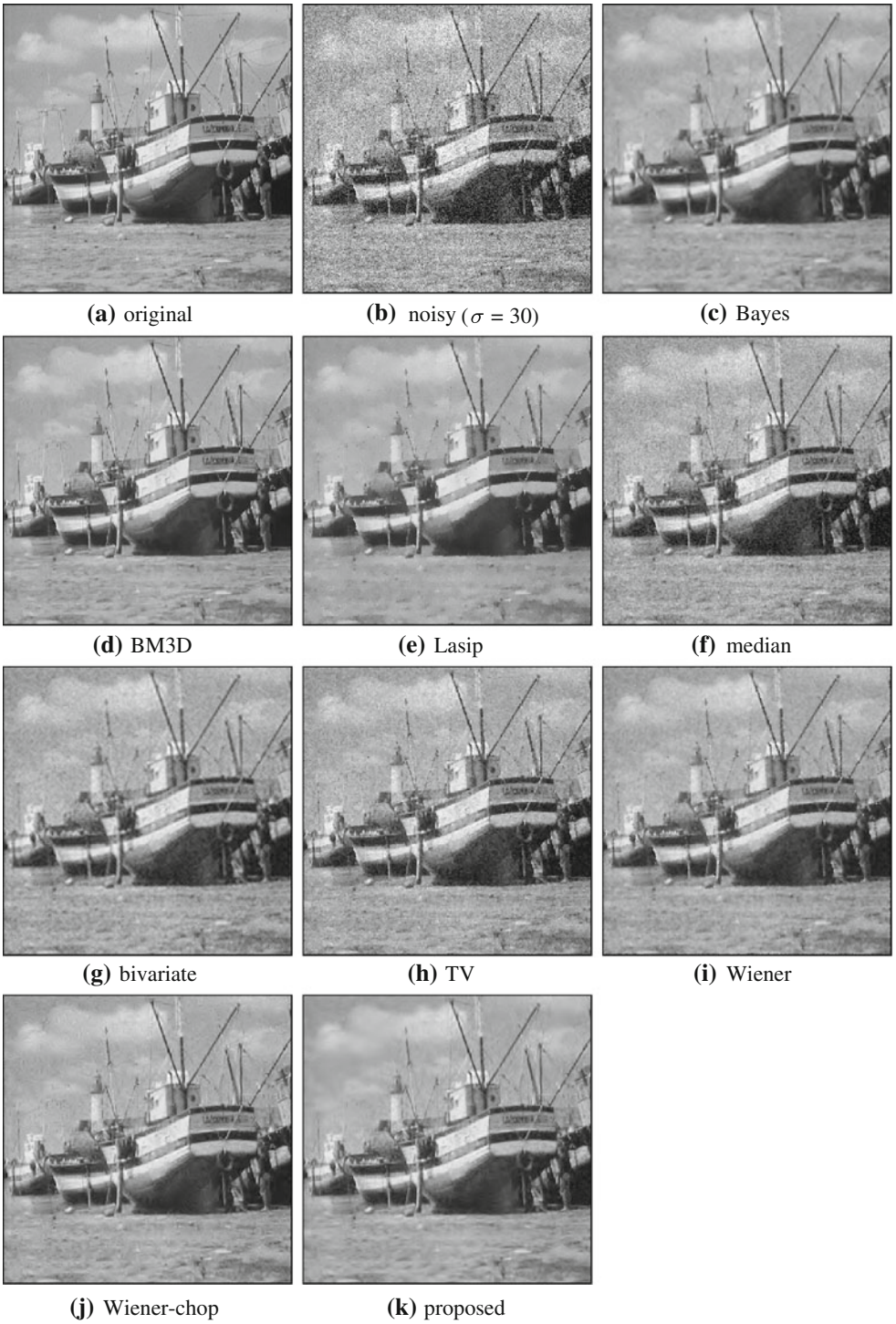


**Fig. 6** Denoising results for image boat

Bayes and Bivariate methods. The proposed method achieves similar results to all approaches considered in the comparison. However, when only wavelet-based approaches are considered, the proposed method achieves better results with PSNR and FOM and is similar to the Wiener-chop method regarding the SSIM measure.

Even though the proposed method is simple in nature, the results are comparable to those obtained with BM3D and superior to AD, TV, median and Wiener. Compared to BM3D, it is worth noticing that, although this method behaves well for lower noise ratios, it experiences a downfall at two higher noises ($\sigma = 30$ and $\sigma = 35$). Differently, the proposed method presents a more linear trend.

Figures 5, 6, 7 and 8 show four original and corresponding noisy images as well as denoised images obtained employing several denoising methods.

Bayes wavelet-based methods tend to produce smoothed results in homogeneous regions. Nevertheless, certain features such as edges are affected. As the proposed denoising method takes into account the located edges in each high-frequency subband to threshold the wavelet coefficients, it is possible to observe that such adaptive thresholding, in conjunction with the block approach, effectively reduces noise while preserving features of the image. This effect can be better seen in Figs. 7k and 8k.

The Wiener-chop method produces a similar result on edges. However, as can be perceived through Figs. 5, 6, 7 and 8, the proposed method outperforms Wiener-chop in homogeneous regions, producing smoother results. That can be clearly seen in the sky region in Fig. 7.

The bivariate, Wiener and TV methods fail to smooth images when noise increases to higher levels. TV produces good results at lower $\sigma$ values but obtains poor denoised images at higher noise levels.

BM3D and AD methods output smoothed images. The worst resulting images are produced at higher levels of noise. The AD method shows a general tendency for oversmoothing which leads to images with an oil painting-like effect, as seen in Figs. 5e and 6e. As stated before, BM3D experiences a sudden fall for PSNR and SSIM measures at higher levels of noise. The images present artifacts in homogeneous regions.

## 5 Conclusions

This paper presented an adaptive edge-preserving image denoising method in wavelet domain. A new thresholding scheme is proposed based on noise estimation on high-frequency subbands and edge strength. The choice of

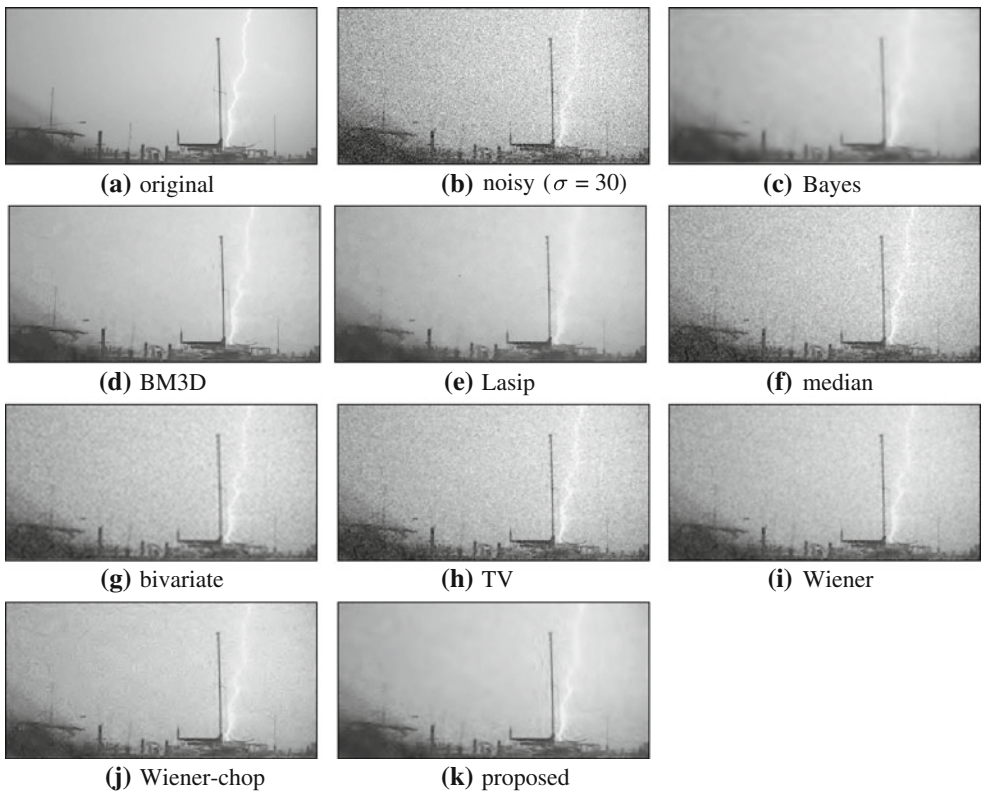


**Fig. 7** Denoising results for image lightning

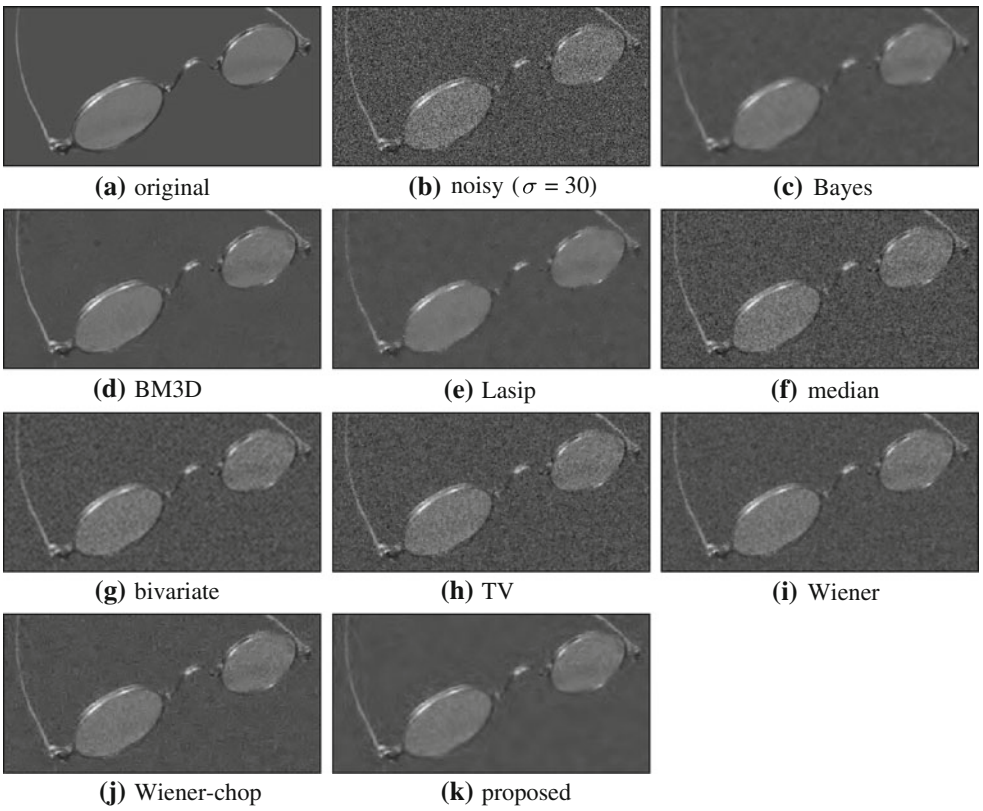


**Fig. 8** Denoising results for image glasses

thresholding functions integrated with edge detection can improve the performance of denoising methods.

Results indicated that the proposed method effectively suppresses Gaussian noise without smoothing important image details. Experiments demonstrated that the new method produces superior results compared to other methods based on the wavelet transform and results comparable to other state-of-the-art denoising methods.

**Acknowledgments** The authors are thankful to FAPESP, CNPq and CAPES for the financial support. This research was partially supported by FAPESP Grant 2010/10618-3.

## References

1. Abreu E, Lighstone M, Mitra S, Arakawa K (1996) A new efficient approach for the removal of impulsive noise from highly corrupted images. IEEE Trans Image Process 5(6):1012–1025
2. Garnett R, Huegerich T, Chui C, He W (2005) A universal noise removal algorithm with an impulse detector. IEEE Trans Image Process 14(11):1747–1754
3. Gonzalez RC, Woods RE (2006) Digital image processing. Prentice-Hall, Upper Saddle River
4. Pitas I, Venetsanooulos A (1990) Nonlinear digital filters: principles and applications, Kluwer, Boston
5. Yüksel M, Bastürk A (2003) Efficient removal of impulse noise from highly corrupted digital images by a simple neuro-fuzzy operator. Int J Electron Commun 57(3):214–219
6. Sethian JA (1999) Level set methods and fast marching methods: evolving interfaces in computational geometry, fluid mechanics, computer vision and materials sciences. Cambridge University Press, Cambridge
7. Chambolle A, Vore RD, Lee NY, Lucier B (1998) Nonlinear wavelet image processing: variational problems, compression, and noise removal through wavelet shrinkage. IEEE Trans Image Process 7(3):319–335
8. Chambolle A (2004) An algorithm for total variation minimization and applications. J Math Imaging Vis 20(1–2):89–97
9. Rudin L, Osher S, Fatemi E (1992) Nonlinear total variation based noise removal algorithms. Phys D 60:259–268
10. Black MJ, Sapiro G, Marimont DH, Heeger D (1998) Robust anisotropic diffusion. IEEE Trans Image Process 7(3):421–432
11. Katkovnik V, Egiazarian K, Astola J (2006) Local approximation techniques in signal and image processing, vol. PM157, SPIE Press, USA
12. Weickert J, ter Haar Romeny BM, Viergever MA (1998) Efficient and reliable schemes for nonlinear diffusion filtering. IEEE Trans Image Process 7(3):398–410
13. Chan TF, Zhou HM (1999) Adaptive ENO-wavelet transforms for discontinuous functions, Technical Report 99-21, Computational and Applied Mathematics Technical Report, Department of Mathematics, UCLA (Jun. 1999)
14. Egiazarian K, Astola J, Helsingius M, Kuosmanen P (1999) Adaptive denoising and lossy compression of images in transform domain. J Electron Imaging 8(3):233–245
15. Dabov K, Foi A, Katkovnik V, Egiazarian K (2006) Image denoising with block-matching and 3D filtering. In: SPIE electronic imaging: algorithms and systems, vol. 6064, pp. 606414–1–606414–12

16. Wongsawat Y, Rao K, Oraintara S (2005) Multichannel SVD-based image denoising. In: IEEE international symposium on circuits and systems, vol 6, pp 5990–5993
17. Orchard J, Ebrahimi M, Wong A (2008) Efficient nonlocal-means denoising using the SVD. In: IEEE international conference on image processing. San Diego, CA, USA, pp 1732–1735
18. Weyrich N, Warhola GT (1998) Wavelet shrinkage and generalized cross validation for image denoising. IEEE Trans Image Process 7(1):82–90
19. Nason GP (1996) Wavelet shrinkage by cross-validation. J R Stat Soc B 58:463–479
20. Chipman H, Kolaczyk E, McCulloch R (1997) Adaptive Bayesian wavelet shrinkage. J Am Stat Assoc 440(92):1413–1421
21. Ruggeri F, Vidakovic B (1998) A Bayesian decision theoretic approach to wavelet thresholding. J Am Stat Assoc 93:173–179
22. Vidakovic B (1998) Nonlinear wavelet shrinkage with bayes rules and bayes factors. J Am Stat Assoc 93(441):173–179
23. Chang S, Yu B, Vetterli M (2000) Spatially adaptive wavelet thresholding based on context modeling for image denoising. IEEE Trans Image Process 9(9):1522–1531
24. Crouse MS, Nowak RD, Baraniuk RG (1998) Wavelet-based statistical signal processing using hidden Markov models. IEEE Trans Signal Process 46(4):886–902
25. Fan G, Xia X (2001) Image denoising using local contextual hidden Markov model in the wavelet domain. IEEE Signal Process Lett 8(5):125–128
26. Liu J, Moulin P (2001) Complexity-regularized image denoising. IEEE Trans Image Process 10(6):841–851
27. Mihcak MK, Kozintsev I, Ramchandran K, Moulin P (1999) Low-complexity image denoising based on statistical modeling of wavelet coefficients. IEEE Signal Process Lett 6(12):300–303
28. Romberg JK, Choi H, Baraniuk RG (1999) Shift-invariant denoising using wavelet-domain hidden Markov trees. In: Conference record of the thirty-third asilomar conference on signals, systems and computers, pacific grove, CA, USA, pp 1277–1281
29. Bao Q, Gao J, Chen W (2008) Local adaptive shrinkage threshold denoising using curvelet coefficients. Electron Lett 44(4):277–279
30. Chang S, Yu B, Vetterli M (2000) Adaptive wavelet thresholding for image denoising and compression. IEEE Trans Image Process 9(9):1532–1546
31. Choi H, Baraniuk R (1998) Analysis of wavelet-domain wiener filters. In: IEEE international symposium on time-frequency and time-scale analysis, Pittsburgh, PA, USA, pp 613–616
32. Donoho DL, Johnstone IM (1994) Ideal spatial adaptation via wavelet shrinkage. Biometrika 81:425–455
33. Donoho DL, Johnstone IM (1995) Adapting to unknown smoothness via wavelet shrinkage. J Am Stat Assoc 90(432):1200–1224
34. Ghael S, Ghael EP, Sayeed AM, Baraniuk RG (1997) Improved wavelet denoising via empirical wiener filtering. In: Proceedings of SPIE, vol 3169. San Diego, CA, USA, pp 389–399
35. Kazubek M (2003) Wavelet domain image denoising by thresholding and wiener filtering. IEEE Signal Process Lett 10(11):324–326
36. Pižurica A, Philips W (2006) Estimating the probability of the presence of a signal of interest in multiresolution single- and multiband image denoising. IEEE Trans Image Process 15(3):654–665
37. Portilla J, Strela V, Wainwright M, Simoncelli E (2003) Image denoising using scale mixtures of gaussians in the wavelet domain. IEEE Trans Image Process 12(11):1338–1351
38. Sendur L, Selesnick IW (2002) Bivariate shrinkage with local variance estimation. IEEE Signal Process Lett 9(12):438–441
39. Weaver J, Yansun X, Cromwell DHL (1991) Filtering noise from images with wavelet transforms. Magn Reson Med 21(2):288–295
40. Malfati M, Roose D (1997) Wavelet-based image denoising using a Markov random field a priori model. IEEE Trans Image Process 6(4):549–565
41. Donoho DL (1995) De-noising by soft-thresholding. IEEE Trans Inf Theory 41(3):613–627
42. Yuan X, Buckles B (2004) Subband noise estimation for adaptive wavelet shrinkage. In: 17th international conference on pattern recognition, vol 4, pp 885–888
43. Donoho DL, Johnstone IM (1998) Minimax estimation via wavelet shrinkage. Ann Stat 26(3):879–921
44. Jansen M (2001) Noise Reduction by wavelet thresholding. Springer-Verlag, New York, USA
45. Antoniadis A (2007) Wavelet methods in statistics: some recent developments and their applications. Stat Surv 1:16–55
46. Gao HY, Bruce AG (1997) WaveShrink with firm shrinkage. Statistica Sinica 7:855–874
47. Gao HY (1998) Wavelet shrinkage denoising using the non-negative garrote. J Comput Graph Stat 7(4):469–488
48. Antoniadis A, Fan J (2001) Regularization of wavelet approximations. J Am Stat Assoc 96(455):939–967
49. Mallat S (1989) A theory for multiresolution signal decomposition: the wavelet representation. IEEE Trans Pattern Anal Mach Intell 11(7):674–693
50. Caltech, Caltech 256 (2011) http://www.vision.caltech.edu/Image_Datasets/Caltech256/images/. Accessed 13 July 2011
51. Wang Z, Bovik A, Sheikh H, Simoncelli E (2004) Image quality assessment: from error visibility to structural similarity. IEEE Trans Image Process 13(4):600–612
52. Pratt W (1978) Digital image processing. Wiley, New York
53. Nason GP, Silverman BW (1995) The stationary wavelet transform and some statistical applications. In: Lecture notes in statistics: wavelets and statistics, Springer-Verlag, Berlin, pp 281–300